Modeling the Reaction Kinetics and Dynamics of the HIF1 Network - Supplement

Over the past 20 years the transcription factor hypoxia inducible factor 1 (HIF1) has been implicated in pathways critical to the cellular response to hypoxic conditions. Interest in HIF1 grew after the discovery of its overexpression within cancerous tumor cells, which are inherently always starved of oxygen. Since then, HIF1 has been found as among the key factors involved in inflammatory pathways[1], with networks that cross talk with mTOR (mammalian target of Rapamycin) and NF-κB (nuclear factor kappa B) respectively.

This clearly demonstrates the need for models of the kinetics and dynamics of the HIF network. The interactions of HIF and its regulatory proteins inside and outside the cytosol are both multifaceted and complex. The nontrivial interactions of varying O_2 concentration over time introduce even more unexpected and complex behavior to the system. Clearly an *in silico* approach that can capture these complex dynamics is warranted, which is presented here.

The Biology of HIF1

Under normoxia conditions, HIFα (the first part of the HIF1 dimer) is produced but immediately degraded by an O_2 dependent pathway. The proteins FIH (factor inhibiting HIF1) and PHD (prolyl hydroxylase) bind oxygen as a substrate to hydroxylate HIF at two positions, which mark it for degradation by a VHD (Von-Hippel Landau degradation) pathway. Under hypoxic conditions however, HIFα is transported into the nucleus, where it can bind with HIF**β** (the second part of the dimer) and form the HIFd complex, this complex then binds to HRE (hypoxia response elements) on DNA and induces transcription.

The Model

Our choice of reactions to model the HIF1 network derives from the Nguyen et. al in 2013[2], who described the HIF/PHD/VHL network as above. We implement the model as a

python program and system of ODE's divided into two compartments, with 29 reactions total (Table S1). Major assumptions we make include that the rates of relevant enzymes are independent of the compartment (ie. that they are equal in both the cytosol and the nucleus. Furthermore O2 binding is assumed to be irreversible and occur only at aryl and prolyl positions, and functions as a "mark" for the VHL degradation pathway, which is assumed to be a single step, mass action kinetic reaction.

Our kinetic parameters are presented in Table S2 below, the Michaelis Menten parameters for oxygen binding to FIH and PHD, as well as the mRNA production rate are experimentally determined from reaction assays done by Hirsila et al., 2003; Koivunen et al., 2007; Kaelin and Ratcliffe, 2008. The remainder of the parameters are set to either physiologically plausible values for protein-protein interactions or fitted to match published experimental data by Nguyen.

To model the transition between normoxia and hypoxia in our simulation, we use relative concentrations of oxygen. At t=0 the concentration is defined to be 100%, then at t>0 we define

$$\text{Hypo3(t)} = \text{O}_2 \cdot \left(1 - \frac{18}{21}\,\text{StepFunction}(t - t_{start})\right)$$

Which uses the discontinuous step function (0 at t = t_start and 1 at t > t_start) to model the change to 3% oxygen level. This was found to be too steep of a transition and also not a physiologically plausible mechanism for oxygen change and was modified to the smoothed sigmoid function with a steepness parameter to control the change to hypoxia.

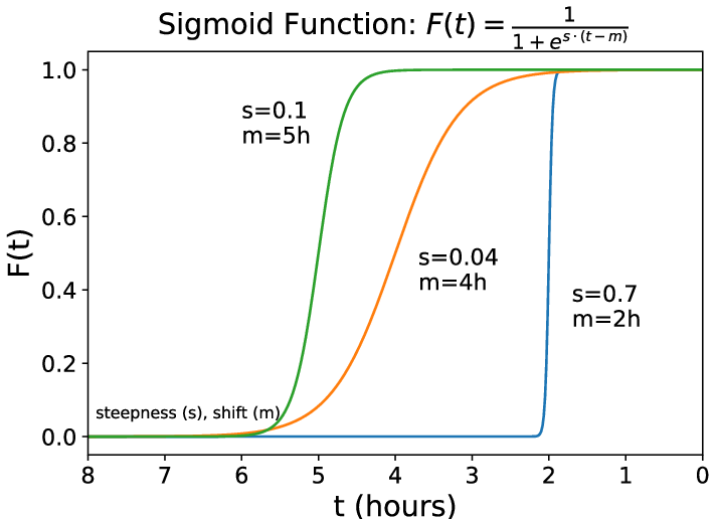

Fig S1. The Sigmoidal function used to model oxygen change.

We implemented three models using the parameters discussed above. The base kinetic reaction network, a stochastic implementation of the previous reaction, and a model incorporating echinomycin as an inhibitor. Echinomycin is a bicyclic, peptide based antibiotic that inhibits HIF1. Its intercalation into DNA prevents the binding of the HIFd dimer to the HRE[5]. Echinomycin's inhibition of HIF1 means it has potential as a cancer therapeutic, with multiple Phase II trials underway.

Results

The simulation was run for a duration of 100 seconds for the kinetic reaction network and 100 hours for the stochastic (Gillespie) model. The end point of the model is a 'Luciferase' species connected to the production of protein induced by HIF1, which was included so that the computational results can be correlated to the Luciferase assay, a common tool used to measure HIF1 activity. Luciferase is a bioluminescent protein whose concentration allows the quantitative measurement of protein expression by recording light intensity.

Our results for the HIFα concentration over time (Fig.2) show the same exponential growth under hypoxia that cells demonstrate. Furthermore the dynamics of the HIFα forming HIF dimer follow the expected curve, where the HIFα concentration spikes after the induction of hypoxia and quickly falls off as the dimer forms. Over time the concentration returns to the steady state equilibrium of dimer and HIFα.

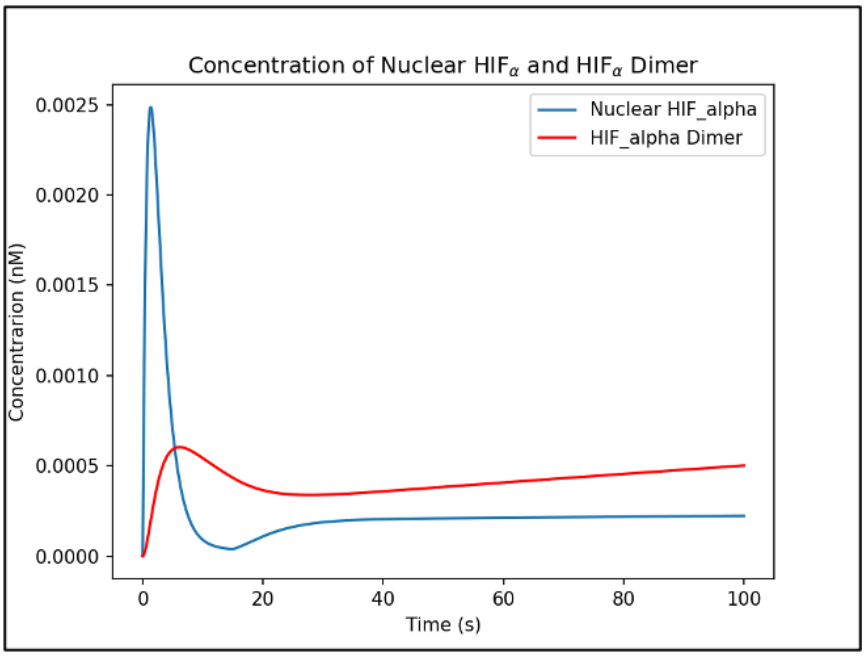

Fig.2 The concentration of nuclear HIFα over time in the deterministic model and its conversion to the HIF dimer.

In the echinomycin model, we model the binding and unbinding reaction of echinomycin to the HRE using the differential equation

$$d[HRE - ECH]/dt = k_{ecf}[ECF][HRE] - k_{ecr}[HRE - ECF]$$

Where HRE-ECH is the echinomycin - DNA complex and the constants describe the forward and reverse (binding / unbinding) reaction respectively.

To determine the active concentration of antibiotic in the model, we vary the echinomycin concentration and run the simulation to steady state, then return the concentration of the HIF-HRE complex(Fig.3A). We choose the midpoint of 35 nM as the inhibiting concentration and plot the trajectory (Fig. 3B). The trajectory shows a clear difference, where even under hypoxic conditions the formation of the HIF-HRE complex is inhibited.

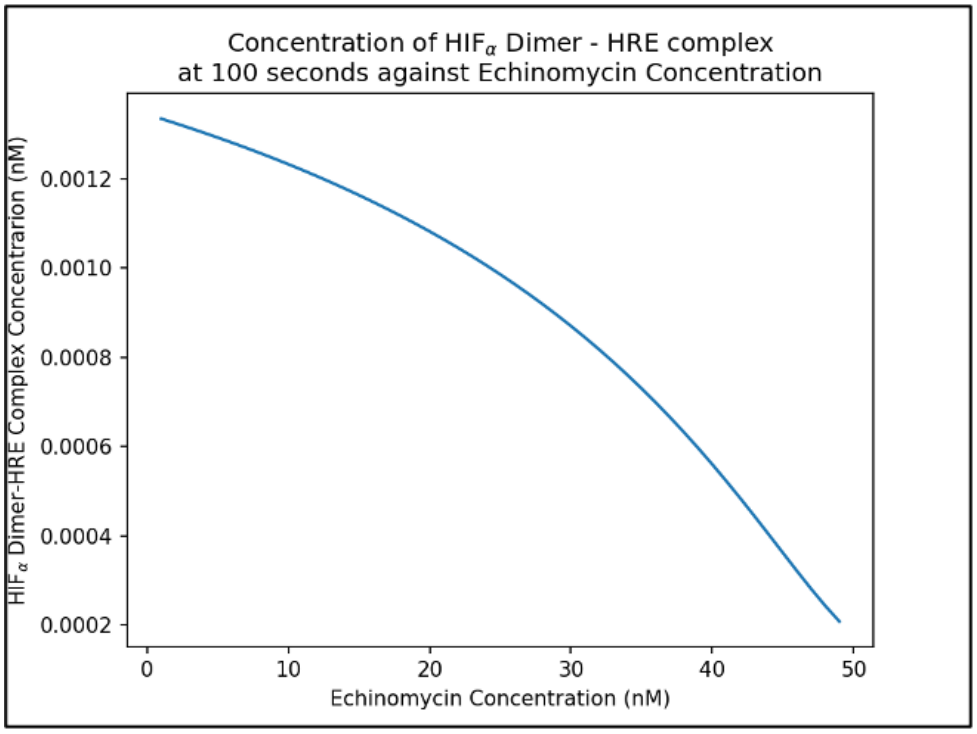

Fig, 3A - The changing steady state concentration of the HIF-HRE complex as a function of echinomycin concentration.

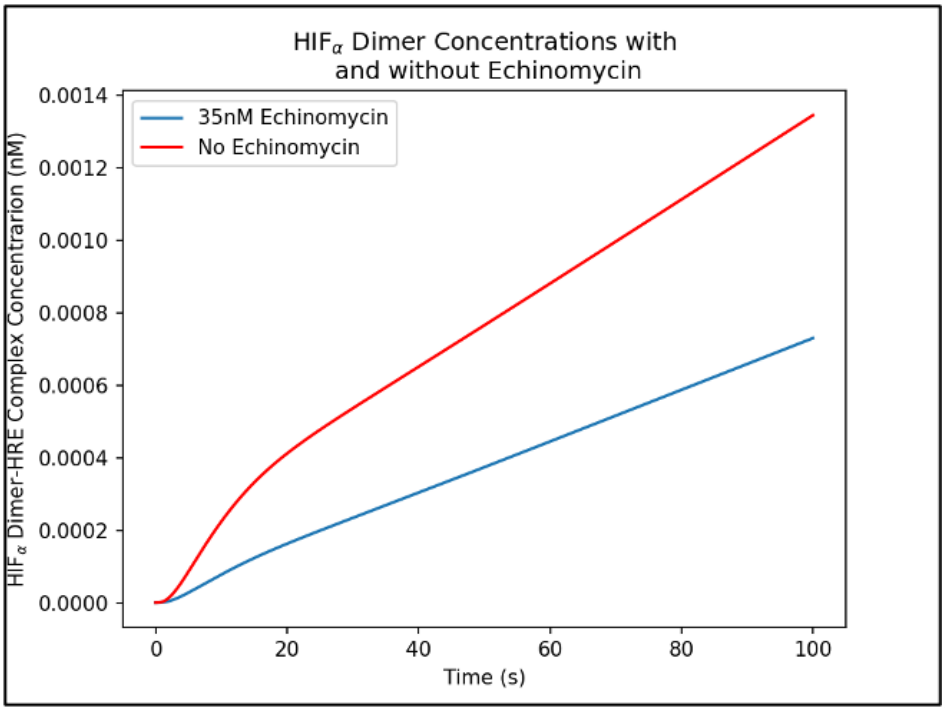

Fig. 3B - The Dimer concentration at 35 nM over time compared to the same trajectory without antibiotic.

Lastly, to further investigate the effects of switching the oxygen concentration to hypoxic conditions, we used a simplified 12 reaction model (below) to capture the core dynamics of the HIF network, with an oxygen switch to start and end hypoxic conditions over a period of hours.

Equation	Reaction description
$\rightarrow HIF\alpha(c)$	HIFα protein production
$HIF\alpha(c) \rightarrow \phi$	HIFα degradation (cytoplasmic)
$HIF\alpha(c) \rightarrow HIF\alpha(n)$	HIFα nuclear import
$HIF\alpha(n) + HIF\beta(n) \leftrightarrow HIF(d)$	HIF dimerization (reversible)
$HIF(d) + HRE \leftrightarrow HIF(d) \cdot HRE$	HIF-HRE binding (reversible)
$HIF(d) \cdot HRE \rightarrow mRNA + HIF(d) \cdot HRE$	Target gene transcription
$mRNA \rightarrow Protein$	Target gene translation
$mRNA \rightarrow \phi$	mRNA degradation
$Protein \rightarrow \phi$	Protein degradation
$HIF\alpha(n) \rightarrow \phi$	HIFα degradation (nuclear)

The results of the trajectories indicated that the control of the reaction pathway is determined by hypoxia and the availability of the oxygen.

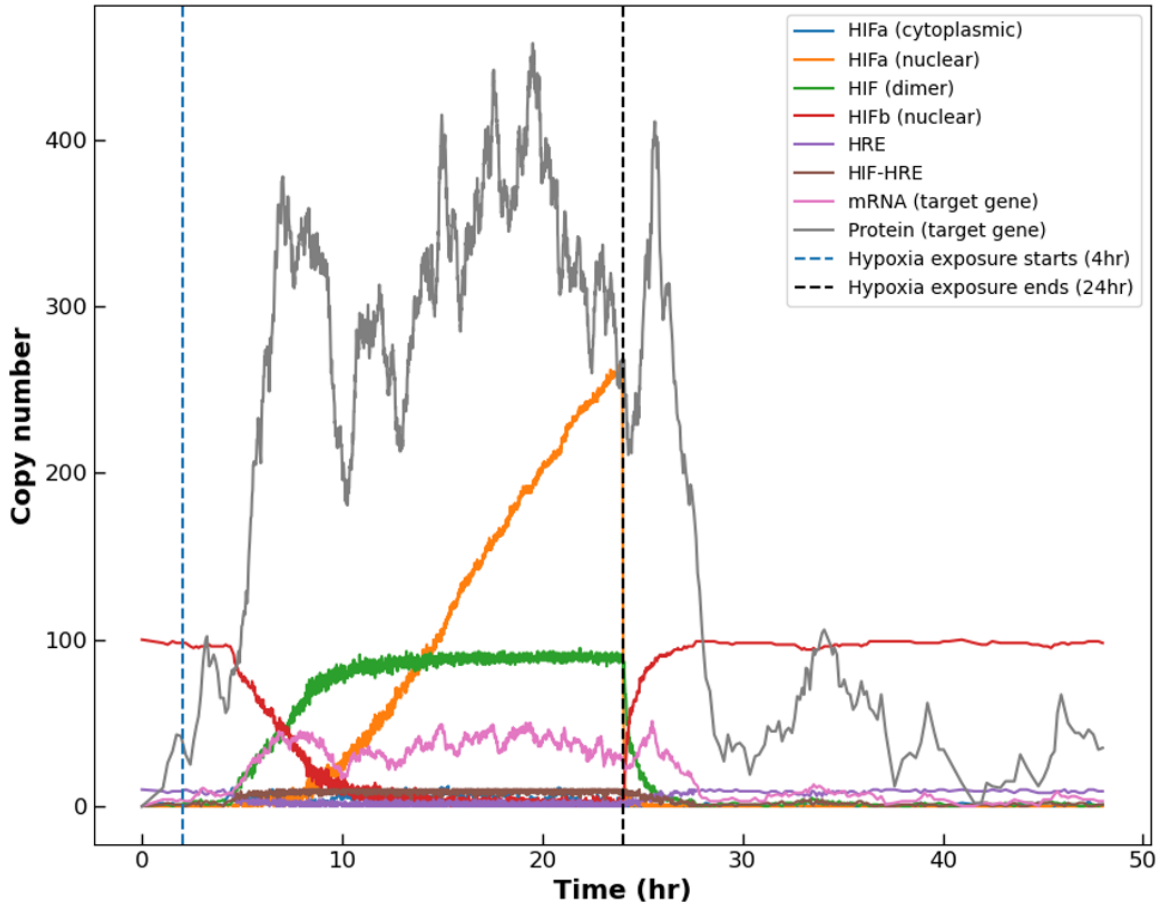

Fig 4 - The trajectory of relevant species using the Gillespie model and the O2 switch. The trajectories clearly demonstrate that the reaction pathway is controlled by O2.

The dashed lines represent the transition to and from hypoxic conditions. We can clearly observe the same qualitative dynamics as the deterministic model. The target gene contraction is dependent on the start and end of hypoxia, and the nuclear HIFa concentration increases until the end hypoxic conditions, where it immediately craters.

The Gillespie data clearly models both the fundamental dynamics of the HIF system captured by the reduced equation set and the switch behavior caused by the onset and end of hypoxic conditions.

References

1. Cavadas, Miguel As, et al. "Hypoxia-Inducible Factor (HIF) Network: Insights from Mathematical Models." *Cell Communication and Signaling*, vol. 11, no. 1, Dec. 2013, p. 42. *DOI.org (Crossref)*, https://doi.org/10.1186/1478-811X-11-42.
2. Fletcher, Michael C., and Keith R. Fox. "Dissociation Kinetics of Echinomycin from CpG Binding Sites in Different Sequence Environments." *Biochemistry*, vol. 35, no. 3, Jan. 1996, pp. 1064–75. *DOI.org (Crossref)*, https://doi.org/10.1021/bi9523623.
3. Murphy, Ryan J., et al. "Growth and Adaptation Mechanisms of Tumour Spheroids with Time-Dependent Oxygen Availability." *PLOS Computational Biology*, edited by Philip K. Maini, vol. 19, no. 1, Jan. 2023, p. e1010833. *DOI.org (Crossref)*, https://doi.org/10.1371/journal.pcbi.1010833.
4. Nguyen, Lan K., et al. "A Dynamic Model of the Hypoxia-Inducible Factor 1-Alpha (HIF-1α) Network." *Journal of Cell Science*, Jan. 2013, p. jcs.119974. *DOI.org (Crossref)*, https://doi.org/10.1242/jcs.119974.
5. Pressley, Mariyah, et al. "Cycling Hypoxia Selects for Constitutive HIF Stabilization." *Scientific Reports*, vol. 11, no. 1, Mar. 2021, p. 5777. *DOI.org (Crossref)*, https://doi.org/10.1038/s41598-021-85184-8.
6. Riboldi, Elena, and Antonio Sica. "Modulation of Innate Immunity by Hypoxia." *The Innate Immune Response to Noninfectious Stressors*, Elsevier, 2016, pp. 81–106. *DOI.org (Crossref)*, https://doi.org/10.1016/B978-0-12-801968-9.00004-0.

7. Semenza, Gregg L. “Targeting HIF-1 for Cancer Therapy.” *Nature Reviews Cancer*, vol. 3, no. 10, Dec. 2003, pp. 721–32. *DOI.org (Crossref)*, https://doi.org/10.1038/nrc1187.
8. Yucel, Meryem A., and Isil Aksan Kurnaz. “An in Silico Model for HIF‐α Regulation and Hypoxia Response in Tumor Cells.” *Biotechnology and Bioengineering*, vol. 97, no. 3, June 2007, pp. 588–600. *DOI.org (Crossref)*, https://doi.org/10.1002/bit.21247.

Table S1/S2 - Reactions, Rates, Constants Implemented in the Model (Nguyen. Et. al. 2013)

	Reactions	Reaction rates
v_1	$\rightarrow$ HIFα	k_1
v_2	HIFα $\rightarrow$ null	$k_2 \cdot \text{HIF}\alpha$
v_3	HIFα $\rightarrow$ HIFα-pOH (catalysed by PHD + O_2)	$k_3 \cdot \text{PHD} \cdot \frac{O_2}{Km_{3a} + O_2} \cdot \frac{\text{HIF}\alpha}{Km_{3b} + \text{HIF}\alpha}$
v_4	HIFα-pOH $\rightarrow$ null (catalysed by VHL)	$k_4 \cdot \text{VHL} \cdot \frac{\text{HIF}\alpha\text{-pOH}}{Km_4 + \text{HIF}\alpha\text{-pOH}}$
v_5	HIFα $\rightarrow$ HIFα-aOH (catalysed by FIH + O_2)	$k_5 \cdot \text{FIH} \cdot \frac{O_2}{Km_{5a} + O_2} \cdot \frac{\text{HIF}\alpha}{Km_{5b} + \text{HIF}\alpha}$
v_6	HIFα-aOH $\rightarrow$ HIFα	$k_6 \cdot \text{HIF}\alpha\text{-aOH}$
v_7	HIFα-aOH $\rightarrow$ HIFα-aOHpOH (catalysed by PHD + O_2)	$k_7 \cdot \text{PHD} \cdot \frac{O_2}{Km_{7a} + O_2} \cdot \frac{\text{HIF}\alpha\text{-aOH}}{Km_{7b} + \text{HIF}\alpha\text{-aOH}}$
v_8	HIFα-aOHpOH $\rightarrow$ null (catalysed by VHL)	$k_8 \cdot \text{VHL} \cdot \frac{\text{HIF}\alpha\text{-aOHpOH}}{Km_8 + \text{HIF}\alpha\text{-aOHpOH}}$
v_9	HIFα $\rightarrow$ $\text{HIF}\alpha_n$	$k_9 \cdot \text{HIF}\alpha$
v_{10}	$\text{HIF}\alpha_n$ $\rightarrow$ HIFα	$k_{10} \cdot \text{HIF}\alpha_n$
v_{11}	PHD $\rightarrow$ PHD_n	$k_{11} \cdot \text{PHD}$
v_{12}	PHD_n $\rightarrow$ PHD	$k_{12} \cdot \text{PHD}_n$
v_{13}	HIFα-aOH $\rightarrow$ $\text{HIF}\alpha_n$-aOH	$k_{13} \cdot \text{HIF}\alpha\text{-aOH}$
v_{14}	$\text{HIF}\alpha_n$-aOH $\rightarrow$ HIFα-aOH	$k_{14} \cdot \text{HIF}\alpha_n\text{-aOH}$
v_{15}	$\text{HIF}\alpha_n$ $\rightarrow$ $\text{HIF}\alpha_n$-pOH (catalysed by PHD_n + O_2)	$k_{15} \cdot \text{PHD}_n \cdot \frac{O_2}{Km_{15a} + O_2} \cdot \frac{\text{HIF}\alpha_n}{Km_{15b} + \text{HIF}\alpha_n}$
v_{16}	$\text{HIF}\alpha_n$-pOH $\rightarrow$ null (catalysed by VHL_n)	$k_{16} \cdot \text{VHL}_n \cdot \frac{\text{HIF}\alpha_n\text{-pOH}}{Km_{16} + \text{HIF}\alpha_n\text{-pOH}}$
v_{17}	$\text{HIF}\alpha_n$ $\rightarrow$ $\text{HIF}\alpha_n$-aOH (catalysed by FIH_n + O_2)	$k_{17} \cdot \text{FIH}_n \cdot \frac{O_2}{Km_{17a} + O_2} \cdot \frac{\text{HIF}\alpha_n}{Km_{17b} + \text{HIF}\alpha_n}$
v_{18}	$\text{HIF}\alpha_n$-aOH $\rightarrow$ $\text{HIF}\alpha_n$	$k_{18} \cdot \text{HIF}\alpha_n\text{-aOH}$
v_{19}	$\text{HIF}\alpha_n$-aOH $\rightarrow$ $\text{HIF}\alpha_n$-aOHpOH (catalysed by PHD_n + O_2)	$k_{19} \cdot \text{PHD}_n \cdot \frac{O_2}{Km_{19a} + O_2} \cdot \frac{\text{HIF}\alpha_n\text{-aOH}}{Km_{19b} + \text{HIF}\alpha_n\text{-aOH}}$
v_{20}	$\text{HIF}\alpha_n$-aOHpOH $\rightarrow$ null (catalysed by VHL_n)	$k_{20} \cdot \text{VHL}_n \cdot \frac{\text{HIF}\alpha_n\text{-aOHpOH}}{Km_{20} + \text{HIF}\alpha_n\text{-aOHpOH}}$
v_{21}	$\text{HIF}\alpha_n$ + HIFβ $\leftrightarrow$ HIF_d	$k_{21f} \cdot \text{HIF}\alpha_n \cdot \text{HIF}\beta - k_{21r} \cdot \text{HIF}_d$
v_{22}	HIF_d + RHE $\leftrightarrow$ HIF_d-HRE	$k_{22f} \cdot \text{HIF}_d \cdot \text{HRE} - k_{22r} \cdot \text{HIF}_d\text{-HRE}$
v_{23}	HIF_d-HRE $\rightarrow$ mRNA	$k_{23} \cdot \text{HIF}_d\text{-HRE}$

v_{24}	HIF_d-HRE → PHD	$k_{24} \cdot HIF_d\text{-HRE}$
v_{25}	PHD → null	$k_{25} \cdot PHD$
v_{26}	mRNA → null	$k_{26} \cdot mRNA$
v_{27}	mRNA → Protein	$k_{27} \cdot mRNA$
v_{28}	Protein → null	$k_{28} \cdot Protein$
v_{29}	Protein → Luciferase	$k_{29} \cdot Protein$

Parameters	Description	Values	References
k_1	Basal HIFα synthesis rate	0.005	Fitted
k_2	Basal HIFα degradation rate	0.0002	Fitted
k_3	Catalytic rate constant for PHD-mediated hydroxylation of HIFα	0.045	Fitted
Km_{3a}	Michaelis-Menten constant for O_2 as a substrate of PHD	250	(Hirsila et al., 2003; Koivunen et al., 2007; Kaelin and Ratcliffe, 2008)
Km_{3b}	Michaelis-Menten constant for HIFα as a substrate of PHD	100	Fitted
k_4	Catalytic rate constant for VHL-mediated degradation of HIFα-pOH	0.1	Fitted
Km_4	Michaelis-Menten constant for VHL-mediated degradation of HIFα-pOH	150	Fitted
k_5	Catalytic rate constant for FIH-mediated hydroxylation of HIFα	0.4	Fitted
Km_{5a}	Michaelis-Menten constant for O_2 as a substrate of FIH	90	(Hirsila et al., 2003; Koivunen et al., 2007; Kaelin and Ratcliffe, 2008)
Km_{5b}	Michaelis-Menten constant for HIFα as a substrate of FIH	20	Fitted
k_6	Catalytic rate constant for de-hydroxylation of $HIF\alpha_n$-aOH	0.001	Fitted
k_7	Catalytic rate constant for PHD-mediated hydroxylation of HIFα	0.003	Fitted
k_8	Catalytic rate constant for VHL-mediated degradation of HIFα-aOHpOH	0.01	Fitted
k_9, k_{10}	HIFα translocation rates from cytoplasm to and from nucleus	0.001, 0.001	Fitted
k_{11}, k_{12}	PHD translocation rates from cytoplasm to and from nucleus	0.0001, 0.0001	Fitted
k_{13}, k_{14}	HIFα-aOH translocation rates from cytoplasm to and from nucleus	0.0002, 0.0001	Fitted
k_{21f}, k_{21r}	Association and dissociation rates of $HIF\alpha_n$ and HIFβ	0.0005, 0.01	Fitted
k_{22f}, k_{22r}	Association and dissociation rates of heterodimer HIF_d and HRE	0.001, 0.01	Fitted
k_{23}	mRNA production rate	0.0016	(Kugel and Goodrich, 2000)
k_{24}	PHD production rate	0.002	Fitted
k_{25}	PHD degradation rate	0.00001	Based on our >20 hrs measured half-life
k_{26}	mRNA degradation rate	0.00038	Based on our ~30 mins measured half-life

k_{27}	Protein production rate	0.009	(Hargrove, 1993)
k_{28}	Protein degradation rate	0.0001	Based on our ~2 hrs measured half-life
k_{29}	Luciferase export rate	0.02	Assumed fast and not rate-limiting, fitted
O_2	Oxygen level at normoxia	100	Based on (Kaelin and Ratcliffe, 2008)
FIH, FIH_n	Concentrations of FIH in cytoplasm and nucleus	110, 40	Based on (Metzen et al., 2003)
VHL, VHL_n	Concentrations of VHL in cytoplasm and nucleus	50	Assumed equal in both compartments